Experimental Determination of the Fate of Rising CO$_2$ Droplets in Seawater

PETER G. BREWER,*
EDWARD T. PELTZER,
GERNOT FRIEDERICH, AND
GREGOR REHDER[†]

Monterey Bay Aquarium Research Institute, 7700 Sandholdt Road, Moss Landing, California 95039

Direct oceanic disposal of fossil fuel CO$_2$ is being considered as a possible means to moderate the growth rate of CO$_2$ in the atmosphere. We have measured the rise rate and dissolution rate of freely released CO$_2$ droplets in the open ocean to provide fundamental data for carbon sequestration options. A small amount of liquid CO$_2$ was released at 800 m, at 4.4 °C, and the rising droplet stream was imaged with a HDTV camera carried on a remotely operated vehicle. The initial rise rate for 0.9-cm diameter droplets was 10 cm/s at 800 m, and the dissolution rate was 3.0 μmol cm^{-2} s^{-1}. While visual contact was maintained for 1 h and over a 400 m ascent, 90% of the mass loss occurred within 30 min over a 200 m ascent above the release point. Images of droplets crossing the liquid−gas-phase boundary showed formation of a gas head, pinching off of a liquid tail, and rapid gas bubble separation and dissolution.

Introduction

The disposal of fossil fuel CO$_2$ in the deep ocean has been discussed (*1*, *2*) as a means of ameliorating greenhouse gas induced climate change (*3*, *4*). Although models of this process have been formulated (*5*, *6*), and laboratory simulations have been carried out (*7*−*9*), there have been few direct oceanic experiments reported (*4*, *10*, *13*). With the availability of advanced Remotely Operated Vehicle (ROV) technology it has now become possible to carry out controlled releases of many chemical species in the deep sea and to observe and measure the processes taking place. In earlier work (*10*) we have reported on the controlled mid-water release of both CH$_4$ and CO$_2$ into contained spaces to form hydrates trapped at depth for imaging. Here we report on the more difficult problem of observing and accurately measuring the behavior of a rising stream of freely released CO$_2$ in order to evaluate the behavior and dissolution rate of droplets in dynamic motion in the open ocean.

An accurate description of the fate of CO$_2$ injected into ocean water is necessary for predicting the behavior of large-scale ocean disposal schemes. At shallow depths (above about 350 m, depending upon the local temperature gradient) CO$_2$ is in the gas phase and will readily dissolve. Below this depth the gas hydrate phase boundary occurs, again dependent on

local P,T conditions, and a shell of CO$_2$-hydrate may be generated (*11*, *12*) which can have profound consequences; and below about 400 m depth the gas−liquid transition occurs. Each of these regimes can have distinct reaction rates and characteristics. The low compressibility of seawater, and the high compressibility of liquid CO$_2$, results in a density ratio reversal at high pressure such that below about 3000 m depth a gravitationally stable release can be achieved (*13*) under typical ocean conditions. Release at depth leads to long oceanic residence times and effective sequestration from the atmosphere (*14*). However, although release at great depth leads to long residence times, the cost and difficulty of this suggests the need for careful evaluation of mid-depth releases (*6*), which may be very effective near deep water mass formation areas.

Laboratory studies have been successful in identifying both the CO$_2$ hydrate phase boundary and the characteristics of the solid hydrate itself (*15*). It is difficult for a laboratory study to investigate the fate of CO$_2$ droplets and bubbles at high pressure and in complex free motion involving changing bubble dynamics and surface film properties. Thus numerical models have been created, and these have lead to differing conclusions.

Holder et al. (*16*) modeled the behavior of a rising CO$_2$ plume in the case of a constantly growing film of solid hydrate. Since CO$_2$-hydrate is more dense than either seawater or liquid CO$_2$ itself, then this would slow the rise rate and eventually cause sinking. Herzog et al. (*5*) modeled the dissolution rate of liquid CO$_2$ without a hydrate film released at depths between 500 and 2000 m. They concluded that if the initial drop radius is less than 1 cm, complete dissolution would occur within less than 200 m ascent from the release point. A detailed set of model calculations incorporating plume dynamics has been carried out (*6*, *17*), and yet no field data exist to compare models against actual observations.

Experimental Section

Our experiments took place at 800 m depth in Monterey Bay, California. The depth was chosen to match plans for an international experiment designed primarily to study plume dynamics of CO$_2$ released in the deep ocean (*18*).

Remotely Operated Vehicle. We used the ROV *Ventana* (*10*), deployed by the RV *Point Lobos* for our work. The viewing system on Ventana used for real-time observation and permanently recording visual images utilizes the digital "high-definition" television format. The system captures images with a specially modified Sony HDC-750 high-definition television camera which digitizes the picture data and formats it to the SMPTE 292M HDTV interface standard with 2:1 interlace. The resolution of the images is 1080 pixels vertically and 1920 pixels horizontally which is about five times the resolution of conventional video. The image data is continually uplinked from the ROV to the ship for display and simultaneously recorded with a Panasonic HD2000 high-definition videotape recorder without any further transcoding steps. Still frame grabs obtained from the 30 frames/s recording were captured (Viewgraphics Corp.) and processed using standard image processing software (Photoshop).

CO$_2$ Release and Imaging. Early work had shown that it was impossible to obtain accurate size data and maintain within the field of view a CO$_2$ droplet cloud that was free to move in all dimensions. Lack of a dimensional reference, effects of the vehicle motions, strong lateral forcing due to local currents, and the similarity of appearance of a droplet of liquid CO$_2$ to the ubiquitous gelatinous marine organisms,

---

* Corresponding author phone: (831)775-1706; fax: (831)775-1620; e-mail: brpe@mbari.org.

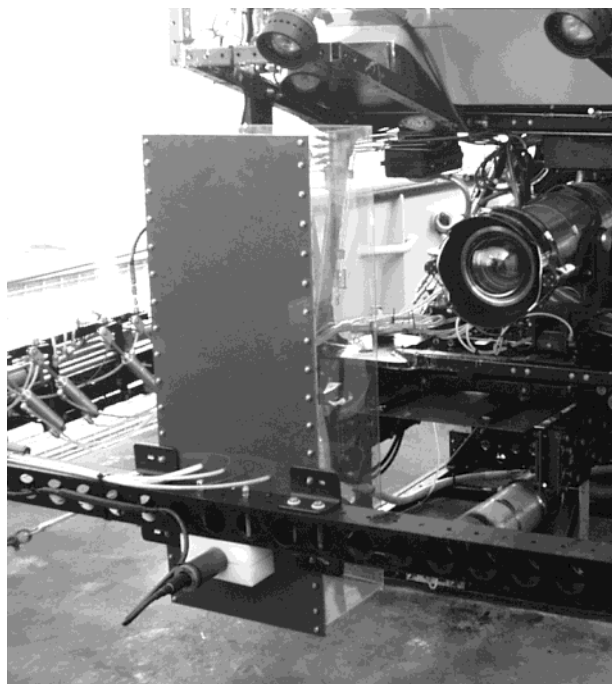† Present address: GEOMAR, Center for Marine Research, Wischhofstrasse 1-3, D-24148, Kiel, Germany.

FIGURE 1. Rear view of the imaging box mounted on a rigid frame in front of the ROV. The HDTV camera is at the right side of the picture. Gas and liquid CO_2 injection lines feed into the back of the box, and below these a pH electrode is mounted on the white block.

all combined to frustrate continuous observation. Therefore we constructed a simple imaging box (Figure 1), 89 cm long, 25 cm deep, and with a transparent face 30 cm wide, open to the ocean at top and bottom, and mounted this directly in the camera field of view. The purpose was to restrain lateral motions, while permitting free upward motion of the droplet plume. The opaque back of the box rejected visual clutter from marine snow in the far field. A meter scale was fixed to the box and was maintained within the imaged field at all times. The injection technique was modified slightly from that described earlier (10) and used a piston assembly, operated by the vehicle hydraulic system, with a displacement capacity of 500 mL. The CO_2 was delivered to the ocean through a 1/8-in. orifice mounted on the back of the imaging box.

While the concept of this experiment is simple, the execution is hard. It requires the precise piloting of a 3 ton vehicle, subject to oceanic forcing in three dimensions, while imaging a small cloud of droplets with millimeter precision for 1 h over hundreds of meters of ascent.

Results

CO_2 in the Liquid Phase. Three experiments were carried out. In the first release the droplet was contained for 21 min, rising from 800 m to 625 m depth, at which time the droplet escaped from the imaging space. In a second release a droplet was followed from 800 m to 340 m depth over a period of about 1 h: the depth versus time curve of the ascent was recorded by the conductivity-temperature-depth (CTD) sensor attached to the vehicle. In Figure 2 we show the temperature profile recorded during the experiments, overlaid on the phase diagram for CO_2 in seawater.

Several droplet release experiments were carried out. For one release a mean ascent rate of 12.8 cm/s was obtained. For another, longer, experiment the mean rise rate was 12.4 cm/s. However, for this experiment the data indicate a measurable increase in velocity with decreasing pressure and diminishing size; the initial rise rate was 10.2 cm/s,
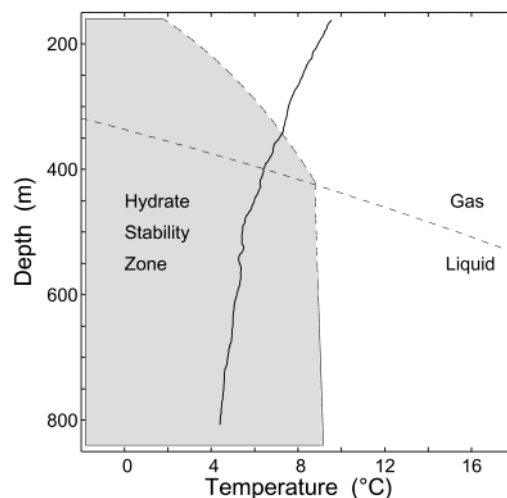

FIGURE 2. The observed ocean temperature profile recorded during the droplet rise experiments, overlaid on the CO_2 phase diagram for seawater at a salinity of 34.

TABLE 1. Measured Liquid CO_2 Droplet Characteristics during Ascent from 800 m Depth[a]

elapsed time (min)	depth (m)	temp (°C)	droplet diameter (cm)		CO_2 density (g/cm³)	amount of CO_2 (millimoles)		rise rate (cm/s)
			(a)	(b)		(a)	(b)	
0	804.5	4.398	0.890		0.9423	7.89		10.2
14.23	706.3	4.740	0.606		0.9310	2.47		11.3
23.13	649.1	4.994	0.485	0.890	0.9235	1.25	7.74	12.0
29.82	602.1	5.165	0.364	0.728	0.9171	0.52	4.21	12.5
43.08	496.8	5.449	0.162	0.647	0.9021	0.05	2.91	13.5
49.73	447.3	5.995		0.364	0.8910		0.51	14.0
61.65	341.2	7.291		0.202	0.8632		0.08	14.9

[a] The initial droplet tracked (a) was joined at about 650 m depth by a second, larger, bubble (b) which became attached. No change in rise rate could be detected due to the attachment, and the changing size of each droplet could be independently determined. The mean density of liquid CO_2 during the rise of the droplets was 0.92 (a) and 0.90 (b), respectively. Thus, a 1 cm³ droplet contains 21.1 (a) or 20.4 (b) millimoles CO_2. We calculate the dissolution rate (Γ) from the slope of

$$(r_t - r_0) = -V_m \times \Gamma \times (t - t_0)$$

where V_m is the specific volume (cm³/mmol), r_0 and r_t are initial droplet radius and droplet radius at time t, and t_0 and t are initial time and the time elapsed since t_0. The observed dissolution rate was 3.0 μmol cm^{-2} s^{-1}.

increasing gradually to 14.9 cm/s at depths shallower than 450 m (Table 1).

The simple picture of a single purely spherical droplet proved unrealistic. It was soon observed that bubble collision was frequent, and we observed rafts of CO_2 droplets that would remain strongly attached to each other for very long periods. It is not known whether a large-scale field release would show such droplet associations. For our work it was necessary to recognize a distinctively shaped unit for following within the droplet cloud. We found such a unit, which formed a droplet pair as shown in Figure 3. The changing dimensions of these droplets during their ascent are given in Table 1. These complex shapes, rotating in three dimensions as they move, presented varying aspect ratios to the camera and frame grabs were carefully selected to remove this effect.

Droplet collision with, and sticking to, the walls of the box did occasionally occur. It was possible to free the droplet with a lateral ROV thruster kick, but because of the possibility of mass loss to the walls, rather than by dissolution, these data were eliminated. The walls of the box inevitably created boundary flow conditions as the vehicle rose, and droplets
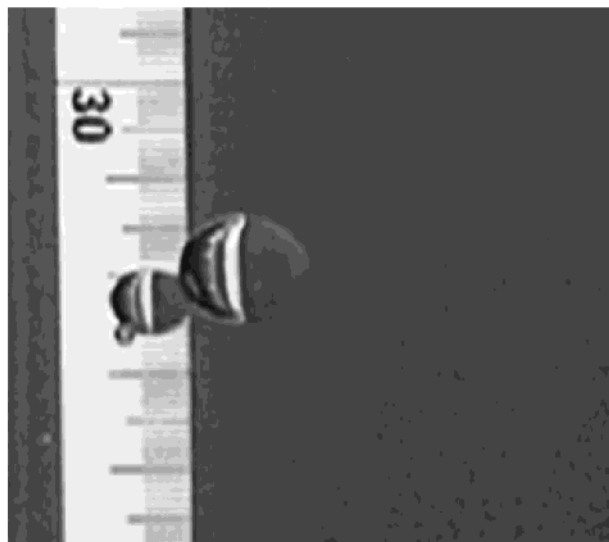
FIGURE 3. Image of the two CO_2 droplets tracked during ascent as they cross the scale (mm divisions). The droplets are in free motion with a mean upward velocity of 12 cm/s. The image was taken from a video frame grab at 654 m depth, 23 min after release.

were consistently drawn to this boundary flow region. Despite these difficulties it proved possible to maintain the droplets in free flow for the ascent, thus any bias due to boundary effects is likely small. This is supported by the smooth rise observed (Figure 4a).

The imaging box was of known dimensions, and a meter scale was attached to the rear wall of the box and always in view. We thus have numerical reference points with which to quantify the size of droplets during ascent. The time at which an image was recorded was logged on the same time base as the vehicle depth (pressure), temperature, etc. Frame grabs from the HDTV videotape were taken at times (shown by the circles in Figure 4a) when the bubble aspect ratio presented to the camera was consistent with long axis view, and droplet dimensions measured with a software cursor compared to the numerical scale. Parallax corrections for the distance between the front and rear walls of the imaging box were made to compensate for differences in imaging the rear mounted scale and the tendency of droplets to migrate to the front of the box, as observed by a second, downward looking, camera.

Also in Table 1 we give the data recorded on droplet size versus depth, and we calculate the mass loss with time. These results show that the droplet diameter changes as a linear function of time and give a dissolution rate for liquid CO_2 of 3.0 μmol cm^{-2} s^{-1} (Figure 4b). We may compare this result, from a rising plume traversing a 8−4 MPa pressure gradient, with the results of Aya et al. (7) from laboratory pressure vessel studies at 30 MPa and 4.5 °C; the laboratory measurements yield a value of 2.8 μmol cm^{-2} s^{-1}. The agreement is excellent given the lower pressures and the higher temperatures involved and the complex fluid dynamics of a rising droplet stream (18).

The Liquid−Gas Transition. In the first releases the transition from liquid droplet to gas bubble could not be observed because of the small droplet size. The data can be smoothly fit with a second order polynomial with no evidence of a discontinuity, although data above this phase boundary are limited. As the droplets rise they shrink because of dissolution, but also expand from pressure decrease, and encounter progressively warmer and less dense seawater as they rise. The net result of this complex process is the small increase in rise rate that we observe.

In a second release the transition region was further explored. In Figure 5 we show an image of this transition:
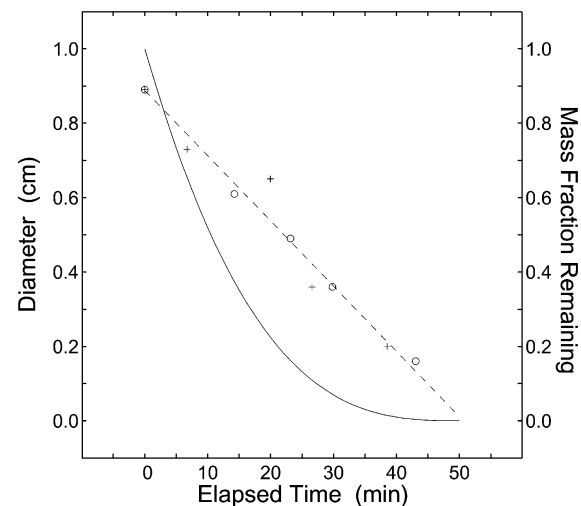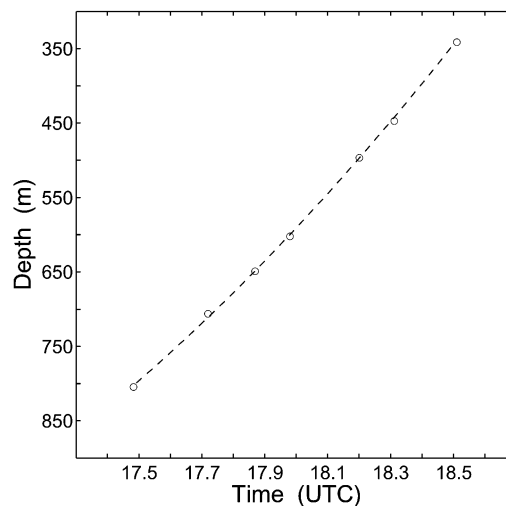

FIGURE 4. (a) Vehicle depth versus time for the experiments reported here. Pressure and temperature are recorded continuously on the vehicle and converted to depth using the seawater equation of state and local gravity. Circles represent locations at which frame grabs were taken for image analysis yielding the data in Table 1. (b) Plot of the changing droplet diameter with time, and remaining mass fraction of the droplets. The droplet size derived from HDTV video analysis, as listed in Table 1, is shown by circles (droplet-a) and pluses (droplet-b), respectively. The dashed line indicates the least-squares fit of eq 1(Table 1); the slope gives a dissolution rate of 3.0 μmol cm^{-2} s^{-1}. The solid line shows the remaining mass fraction relative to the initial mass of the CO_2 droplets.

this illustrates the processes at work. At 400 m the droplet becomes opaque, possibly due to the formation of nascent CO_2 gas, with a hydrate skin, on the droplet surface. A clear "head" of the emergent gas then forms, pushing through the hydrate shell. The buoyant effect of the gas head stretches the remnant liquid droplet, creating a neck. This pinches off, the gas bubble accelerates upward, and the droplet lags behind.

Note that in this oceanic region both gas and liquid phases are within the hydrate phase boundary. In other regions (Mediterranean Sea, Sargasso Sea) warmer deep water depresses the hydrate phase boundary and differing processes may occur.

Presence of a Hydrate Shell. In earlier work (10, 13) we have demonstrated that within the appropriate phase boundary CO_2 clathrate hydrate forms readily, almost instantaneously, on vigorous mixing of CO_2 and seawater. Gas hydrate formation is often recognizable by a change in

FIGURE 5. CO₂ droplet evolution in crossing the liquid−gas-phase boundary, while still within the hydrate stability zone.

optical reflectivity of the surface and by a white cloudy appearance. However, when formed by liquid−liquid contact a pure, transparent, solid is formed. Evidence here of the stiffness of the liquid droplet surface, and its spherical shape, formed immediately after injection, clearly indicate the presence of a hydrate skin. Conditions in the delivery tube promoted hydrate formation, and droplet rafts formed and maintained a stick like shape immediately after release; as the droplets rose they became more rounded. Other work in our laboratory strongly supports the hydrate skin phenomenon. We have carried out similar studies of the fate of a hydrate-forming methane plume in seawater and compared this directly with argon as a comparative, nonhydrate forming, gas (19). The results showed that the presence of a hydrate film reduced CH_4 dissolution rates by a factor of 4, and this is supported for CO_2 by laboratory studies of dissolution rates (7). Holder et al. calculate a reduction in dissolution rate of a factor of 3 for CO_2 released at 1000 m depth (20).

The standard model for both gas (21) and solid (22) dissolution rates in the ocean invokes saturated boundary theory, and we may expect this also to apply to liquid-hydrate-liquid interactions. For velocities of 8 cm/s diffusive boundary layers of about 500 μm are reported (22), and we estimate boundary layer dimensions close to 300 μm for the 12 cm/s rise rates observed in our experiments. Thus the rates observed here at relatively shallow ocean depths may be extended by calculating saturation values in equilibrium with the hydrate at different P,T values. Laboratory saturation data are available (7), and values may also be readily calculated (Multiflash, Infochem Ltd.); from these results we find that dissolution rates at depth should be no more than a factor of 2 slower than those reported here.

Modeling the Rising Behavior of Liquid CO₂ Droplets. Now that we have measured the dissolution rate of liquid CO_2 under upper ocean conditions and rising at an appropriate velocity, we can construct a simple, iterative, numerical model of the released CO_2 droplet based upon the buoyancy of a rigid sphere. As a first approximation to the rise rate of the droplets we use the Stokes velocity, which is the result of a force balance and is applicable for low Reynolds number. Although the Reynolds number in this case is much

higher (100 < Re < 450), the fact that the droplets are covered by a hydrate shell makes their behavior more like a rigid sphere than a fluid or gas bubble. Thus, the Stokes equation is employed, and this assumption will be evaluated by comparing the model and experimental data.

We release a droplet of predetermined size at some depth and temperature, then follow it upward in a stepwise calculation. Acceleration is assumed to be instantaneous, and the upward velocity is determined by the spherical buoyancy equation (16)

$$U = [8gr(\rho_{sw} - \rho_{CO2}/(3\rho_{CO2})]^{0.5} \qquad (1)$$

where assuming a drag coefficient of 1, U is the terminal rise velocity for a rigid sphere, g is the acceleration of gravity, r is the droplet/sphere radius and ρ_{sw} and ρ_{CO2} are the changing in situ densities of seawater and liquid CO_2, respectively.

After a suitably short time interval chosen to give high resolution and precision, we calculate the droplet's new position (depth) and determine seawater density (23) based upon the ambient pressure (computed for this depth) and temperature (obtained from the local temperature gradient) at this point. For this first approximation of a droplet rise model, we interpolated the density of liquid CO_2 from tabulated values for pure CO_2 at 0 °C and 10 °C (24). The remaining mass is calculated based upon the measured dissolution rate (above) and the droplet size. The new droplet size is then determined from the remaining mass and computed density, and a new upward velocity is computed. This process is repeated until the droplet reaches 500 m at which point liquid CO_2 at 10 °C becomes a gas.

The results of this model are shown in Figure 6. We begin by choosing the release depth and droplet size as observed in our experiment. Our objective is to numerically simulate or predict the droplet behavior. In Figure 6a we see that the predicted depth/rise rate of the liquid CO_2 droplet, exactly matches the observed release. Likewise, in Figure 6b, we see that the predicted droplet size and mass fraction remaining are also a good match to the experimentally obtained data.

By comparing predictions with experimental data the Stokes velocity seems to be adequate in this case. The main reason for this appears to be that the droplets are covered with a hydrate shell, and therefore they behave as quasi-solid spheres. It is also interesting to note that while this model is based solely upon the behavior of pure CO_2, it is likely that in the oceanic environment that the CO_2 droplet was rapidly equilibrated with seawater and quickly became saturated with water. Any effect that the saturation of liquid CO_2 with water had on either the rise rate or the dissolution rate was obviously small. Indeed, in Table 2, we see that the calculated solubility of water in liquid CO_2 at the relevant temperatures and pressures is vanishingly small and has little impact on the density so the choice of pure CO_2 as the modeled substance was reasonable.

Discussion

Ocean disposal of CO_2 is but one sequestration option, and within the oceanic realm there are many schemes to be considered. Taken broadly these can include either rising or sinking plumes, with modifications to include hydrate formation, neutralization, etc.

The results obtained here should allow a more accurate prediction of the CO_2/pH field, and the environmental effects, surrounding an injection point.

So far we have considered the droplet plume as having the properties of pure CO_2. However, additional components are very possible, for example, absorption of water and nonpolar species into the CO_2 and surface adsorption of material. Surface adsorption onto bubbles is well-known in the gas transfer literature as the "dirty bubble" problem (25).
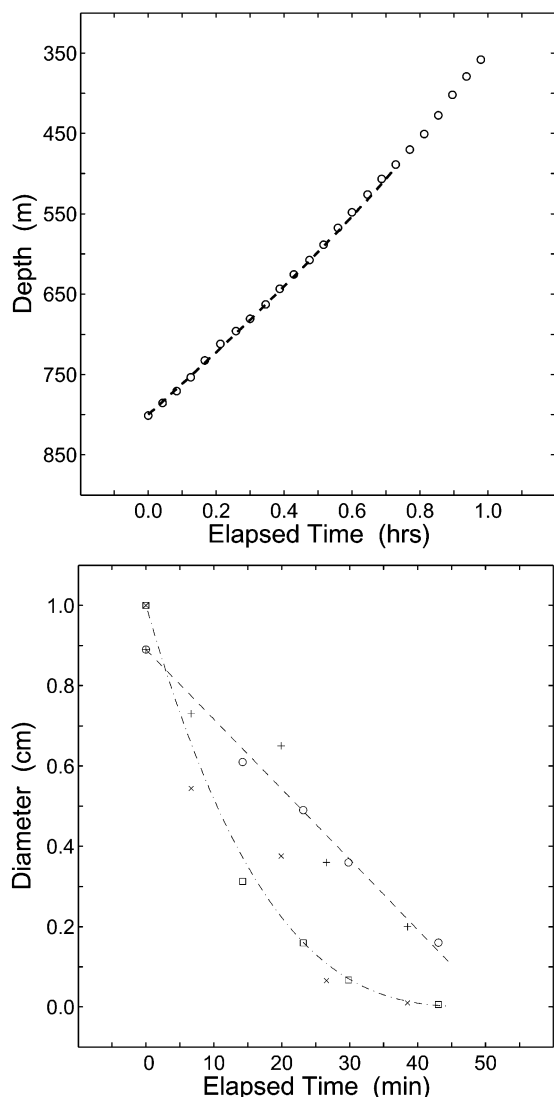
FIGURE 6. Results of the rising droplet model calculations plotted against the observed behavior of liquid CO2. (a) Position of the rising droplet (dashed line) versus the actual ROV depth (circles) at 2.5 min intervals. (b) Modeled droplet diameter (dashed line) and modeled mass fraction remaining (dot−dash line) versus the data for droplet-a (circles and squares) and droplet-b (pluses and crosses), respectively.

TABLE 2. Calculated H_2O Solubility in Liquid CO_2 and Density of Liquid CO_2[a]

depth (m)	Hyd P (dbar)	Abs P (MPa)	temp (°C)	% H_2O (mole)	density of CO_2 pure (g/cm³)	$+ H_2O$ (g/cm³)
400	403.5	4.136	6.42	0.0021	0.89251	0.89254
500	504.5	5.146	5.44	0.0019	0.90992	0.90995
600	605.5	6.157	5.18	0.0017	0.92051	0.92053
700	706.6	7.167	4.76	0.0016	0.93086	0.93088
800	807.7	8.179	4.41	0.0015	0.93992	0.93993

[a] The solubility of water in liquid CO_2 and the density of liquid CO_2 was calculated for five depths and the appropriate ambient temperature conditions using Multiflash software (Infochem Computer Services Ltd, London). Water solubility in liquid CO_2 at these conditions was calculated using the RKSA-infochem model which includes the formation of CO_2 clathrate hydrate as the solubility limiting condition. Subsequently, the liquid CO_2 density was calculated, either for the pure liquid or for the water saturated liquid CO_2 using the Multiflash implementation of the LKP equation of state. As can be seen in the table, the density differences are very small, on the order of 0.00001−0.00003 g/cm³, and are probably not significant within the capabilities of the model.

density that would result from large scale releases, such as "peeling" (or sinking of fingers of dense CO_2 saturated seawater) of the plume due to large-scale fluid dynamic effects (*18*). It is possible to extend these small-scale studies to include biological effects (*28*), and this work is in progress.

Literature Cited

(1) U.S. Department of Energy. *Carbon Sequestration Research and Development*; Oak Ridge National Lab.: 1999.
(2) Brewer, P. G. *Oceanography* **2000**, *13*, 84.
(3) Marchetti, C. *Climate Change* **1977**, *1*, 59.
(4) Handa, N.; Ohsumi, T. *Direct Ocean Disposal of Carbon Dioxide*; Terra Scientific Publishing: Tokyo, 1995; p 274.
(5) Herzog, H.; Golomb, D.; Zemba, S. *Environ. Prog.* **1991**, *10*, 64.
(6) Drange, H.; Alendal, G.; Johannessen, O. M. *Geophys. Res. Lett.* **2001**, *28*, 2637.
(7) Aya, I.; Yamane, K.; Nariai, H. *Energy* **1997**, *22*, 263.
(8) Hirai, S.; Okasabi, K.; Tabe, Y.; Hijikata, K.; Mori, Y. *Energy* **1997**, *22*, 285.
(9) Shindo, Y.; Hakuta, T.; Fujioka, Y.; Koiyama, H. *Energy Convers. Manage.* **1995**, *36*, 479.
(10) Brewer, P. G.; Orr, F. M.. Jr.; Friederich, G.; Kvenvolden, K. A.; Orange, D. L. *Energy Fuels* **1998**, *12*, 183.
(11) Sloan, E. D., Jr. *Clathrate Hydrates of Natural Gases*, 2nd ed.; Dekker: New York, 1998.
(12) North, W. J.; Blackwell, V. R.; Morgan, J. J. *Environ. Sci. Technol.* **1998**, *32*, 676.
(13) Brewer, P. G.; Friederich, G.; Peltzer, E. T.; Orr, F. M., Jr. *Science* **1999**, *284*, 943.
(14) Orr, J. C. et al. *Greenhouse Gas Control Technologies*; Elsevier Science: 2000; Vol. 2.
(15) Sum, A. K.; Burruss, R. C.; Sloan, E. D., Jr. *J. Phys. Chem. B* **1997**, *101*, 7371.
(16) Holder, G. D.; Cugini, A. V.; Warzinski, R. P. *Environ. Sci. Technol.* **1995**, *28*, 276.
(17) Alendal, G.; Drange, H. *J. Geophys. Res.* **2001**, *106*, 1085.
(18) Adams, E.; Akai, M.; Golmen, L.; Haugan, P. M.; Herzog, H.; Masuda, S.; Masutani, S.; Ohsumi, T.; Wong, C. S. In G*reenhouse Gas Control Technologies;* Elsevier: 1999; p 293.
(19) Rehder, G.; Brewer, P. G.; Peltzer, E. T.; Friederich, G. *Geophys. Res. Lett.* **2002**, *29*(15), doi: 10.1029/2001GL013966.
(20) Holder, G. D.; Warzinski, R. P. *Prepr. Pap. Am. Chem. Soc. Div. Fuel Chem.* **1996**, *41*(4), 1452.
(21) Broecker, W. S.; Peng, T.-H. *Tracers in the Sea*; Eldigio Press: 1982.

However, we saw no evidence of this affecting droplet behavior other than the hydrate film itself, even though our experiments took place in a biologically rich environment.

A critical property for the longer term will be the effectiveness of this form of sequestration. For example the depths chosen here cover the 27.3−26.8 (σ_θ) isopycnal (constant potential density) surfaces. The 26.8 surface is the most dense seawater to outcrop seasonally at the surface in the North Pacific, and the ventilation age of this surface has been mapped by Warner et al. (*26*). This probably represents the shallowest depth at which disposal in this ocean basin is likely to be effective. The strong density increase created in CO_2 saturated seawater at relatively shallow depths can lead to sinking plumes, and such disposal scenarios have been elegantly considered (*27*) for North Atlantic sites.

The small-scale ROV experiments described here appear to offer an effective way to evaluate these processes, without the cost and environmental permit requirements for large-scale releases. We are not able with these small quantities to easily simulate some of the changes in local seawater

(22) Santschi, P. H.; Anderson, R. T.; Fleisher, M. Q.; Bowles, W. *J. Geophys. Res.* **1991**, *96*, 10, 641.

(23) Millero, F. J.; Poisson, A. *Deep-Sea Res.* **1981**, *28A*, 625.

(24) Perry, J. H., Ed. *Chemical Engineers' Handbook*, 3rd ed.; McGraw-Hill: New York, 1950; p 206.

(25) Clift, R.; Grace, J. R.; Weber, M. E. *Bubbles, Drops and Particles*; Academic Press: New York, 1978.

(26) Warner, M. J.; Bullister, J. L.; Wisegarver, D. P.; Gammon, R. H.; Weiss, R. F. *J. Geophys. Res.* **1996**, *101*, 20 525.

(27) Haugan, P.; Drange, H. *Nature* **1992**, *357*, 318.

(28) Tamburri, M. N.; Peltzer, E. T.; Friederich, G. E.; Aya, I.; Yamane, K.; Brewer, P. G. *Mar. Chem.* **2000**, *72*, 95.